

S. Boretius  
O. Natt  
T. Watanabe  
R. Tammer  
L. Ehrenreich  
J. Frahm  
T. Michaelis

## In vivo diffusion tensor mapping of the brain of squirrel monkey, rat, and mouse using single-shot STEAM MRI

Received: 10 May 2004  
Revised: 31 August 2004  
Accepted: 16 September 2004  
Published online: 1 December 2004  
© ESMRMB 2004

S. Boretius (✉) · O. Natt · T. Watanabe  
J. Frahm · T. Michaelis  
Biomedizinische NMR Forschungs  
GmbH am Max Planck Institut für  
biophysikalische Chemie,  
37070 Göttingen,  
Germany  
E-mail: sboreti@gwdg.de,  
Tel.: +49-551-2101728  
Fax: +49-551-2101307

R. Tammer · L. Ehrenreich  
Abteilung Neurobiologie,  
Deutsches Primatenzentrum GmbH,  
37077 Göttingen,  
Germany

**Abstract** The purpose was to assess the potential of half Fourier diffusion-weighted single-shot STEAM MRI for diffusion tensor mapping of animal brain in vivo. A STEAM sequence with image acquisition times of about 500 ms was implemented at 2.35 T using six gradient orientations and  $b$  values of 200, 700, and 1200 s mm<sup>-2</sup>. The use of half Fourier phase-encoding increased the signal-to-noise ratio by 45% relative to full Fourier acquisitions. Moreover, STEAM-derived maps of the relative anisotropy and main diffusion direction were completely free of susceptibility-induced signal losses and geometric distortions. Within measuring times of 3 h, the achieved resolution varied from

600×700×1000 μm<sup>3</sup> for squirrel monkeys to 140×280×720 μm<sup>3</sup> for mice. While in monkeys the accessible white matter fiber connections were comparable to those reported for humans, detectable fiber structures in mice focused on the corpus callosum, anterior commissure, and hippocampal fimbria. In conclusion diffusion-weighted single-shot STEAM MRI allows for in vivo diffusion tensor mapping of the brain of squirrel monkeys, rats, and mice without motion artifacts and susceptibility distortions.

**Keywords** Magnetic resonance imaging · Diffusion-weighted imaging · Anisotropy · White matter · Animal brain

### Introduction

Scientific and clinical interest in mapping diffusion properties originally stems from observations of apparent diffusion coefficient (ADC) changes in animal models of cerebral ischemia and in human acute stroke. Subsequently, Moseley et al. [1] and Chenevert et al. [2] demonstrated in cat and human brain, respectively, that the molecular mobility of water in brain tissue exhibits a pronounced directional dependence which mainly originates from the macroscopic, cellular, and subcellular structures of white matter. Because diffusion processes are strongly facilitated along the elongated axon, the ADC turns out to be significantly higher parallel to the direction of a nerve fiber than in directions perpendicular to it. A prominent description of this anisotropic movement of water

molecules uses the concept of the diffusion tensor [3]. In order to map its properties by MRI, it is necessary to record diffusion-weighted (DW) images in at least six different directions as well as one image without or with only a minor diffusion encoding. The resulting data of such a diffusion tensor imaging (DTI) study promises a non-invasive visualization of the axonal integrity, the degree of myelination, and major fiber connections in the individual brain [4, 5].

Despite considerable interest in DTI techniques suitable for laboratory animals, for example with regard to in vivo studies of axonal development or for monitoring the course of neurodegenerative disorders and associated therapies, the acquisition and visualization of diffusion anisotropy in small brains is a persistent challenge. Main difficulties are related to (1) the required resolution

due to the relatively smaller dimensions of nerve fiber bundles than in human brain, (2) the control of involuntary motion (or diffusion-enhanced image ghosting), and (3) the presence of structural susceptibility differences. The latter effect turns out to be much more pronounced in rodents than in humans and therefore poses severe limitations when acquiring DW images with gradient-echo sequences such as echo-planar imaging (EPI). To solve the first two problems, many diffusion studies of animal brain have hitherto been carried out *ex vivo* [6–11]. The absence of motion not only offers long measurement times of up to 24 h [8] but, even more importantly, enables the use of DW spin-echo MRI sequences which are sensitive to motion. On the other hand, because spin-echo sequences do not suffer from susceptibility artifacts, they are applicable at high magnetic field strengths of 7.0–9.4 T. *In vivo* applications of diffusion tensor mapping have been reported for the brain of non-human primates [12, 13], rats [14, 15], and mice [16, 17]. The used magnetic field strengths ranged from 1.5–7.0 T and the measurement times were restricted to 2–3 h.

The purpose of the present work was to introduce a DW single-shot STEAM MRI sequence [18] with half Fourier phase-encoding for studies of animal brain *in vivo*. The approach attempts to combine the main advantages of the two MRI techniques previously applied for *ex vivo* and *in vivo* DTI: similar to EPI, single-shot STEAM MRI overcomes the sensitivity to residual movements even when respective phase errors become enhanced in the presence of strong diffusion-encoding gradients, and similar to spin-echo MRI, the use of stimulated echoes refocuses and thereby eliminates any sensitivity to resonance offset effects (e.g., caused by tissue susceptibility differences). The new method was applied to the brain of squirrel monkeys, rats, and mice.

## Materials and methods

### Animals

Animal fixation and coil arrangements for radiofrequency (RF) excitation and signal detection were optimized separately for each species as shown in Fig. 1. For mice anesthesia was induced by an *i.p.* injection of xylazine (12.5 mg kg<sup>-1</sup> body weight), ketamine (125 mg kg<sup>-1</sup> body weight), and atropine (0.08 mg kg<sup>-1</sup> body weight). In contrast, rats were anesthetized using 2.0–4.0% halothane in a 70:30 mixture of N<sub>2</sub>O/O<sub>2</sub>. Subsequently, both mice and rats were intubated, artificially ventilated, and anesthetized with halothane (1.0–1.5%) in a 70:30 mixture of N<sub>2</sub>O/O<sub>2</sub>. For further details see [19, 20]. Squirrel monkeys received a barbiturate injection (25–35 mg kg<sup>-1</sup> body weight). In all cases the body temperature was monitored by a rectal thermometer and maintained by warm water circulating in two arrays of tubes covering the animal. Breathing was controlled by monitoring a signal derived from a pressure transducer

fixed to the animal's chest. All studies were performed in accordance with German animal protection laws and approved by the responsible governmental authority.

For MRI of the relatively large heads of squirrel monkeys a home-built Helmholtz coil (100 mm inner diameter) for RF excitation and signal reception was found to be appropriate. Rats were studied with use of a birdcage coil (154 mm inner diameter) for RF excitation and a saddle-shaped receive-only surface coil (both Bruker Biospin, Ettlingen, Germany). Mouse brain studies employed a 100-mm Helmholtz coil for RF excitation in conjunction with a circular surface coil (16 mm inner diameter) for signal reception.

### Theoretical considerations

Figure 2 shows a basic RF and gradient scheme of the DW STEAM MRI sequence without spoiler gradients. The method combines a DW spin-echo preparation with a single-shot STEAM imaging module, for further details see [18]. In comparison with EPI, STEAM MRI has a reduced signal-to-noise ratio (SNR). This is because a stimulated echo (STE) refocuses only half of the transverse magnetization of a comparable spin echo, and secondly, because the flip angle  $\alpha$  of the readout RF pulse is limited to avoid a broadening of the point-spread function (PSF). In fact, it should be noted that in EPI a similar PSF broadening by the pronounced T<sub>2</sub>\* decay of the gradient-echo train is usually ignored.

In order to compensate for some of the SNR penalty in DW STEAM MRI, the use of full Fourier (FF) and centrically reordered phase-encoding may be replaced by a half Fourier (HF) scheme [21, 22]. For FF, the amplitudes of two neighboring lines in *k*-space differ by a factor of  $[\cos \alpha \cdot \exp(-TR/T_1)]^2$ . A higher flip angle  $\alpha$  not only leads to larger echo amplitudes of the central *k*-space lines but also broadens the resulting PSF. In fact, the full width at half-maximum in the phase-encoding direction  $FWHM_{ph}$  is given by [18]

$$FWHM_{ph} = \frac{2}{\pi} FOV_{ph} \left( \frac{TR}{T_1} - \ln \cos \alpha \right) \quad (1)$$

where  $FOV_{ph}$  is the field-of-view in the phase direction. In other words, for a fixed  $FWHM_{ph}$  there is a maximum possible flip angle. Conversely, HF schemes acquire only half of the *k*-space acquisitions except for a few central lines needed for phase correction. Accordingly, an ascending phase-encoding scheme which starts in the center of *k*-space leads to amplitudes of neighboring *k*-space lines which differ by only  $\cos \alpha \cdot \exp(-TR/T_1)$ . Because this reduces the resulting  $FWHM_{ph}$  by a factor of 2, the flip angle (and resulting signal strength) can be increased while simultaneously reducing the acquisition time. In addition, the gained time may be invested in a reduced receiver bandwidth to further increase the SNR. Thus, the SNR depends on the flip angle  $\alpha$  (as determined by the desired PSF), the number  $N_p$  of excitations (or phase-encoding steps), and the receiver bandwidth per pixel  $bw$  (or the acquisition time  $1/\sqrt{bw}$ ) according to

$$SNR \sim \sin(\alpha) \sqrt{\frac{N_p}{bw}} \quad (2)$$

**Fig. 1** Animal positioning and coil setup for in vivo MRI studies of the brain of a squirrel monkey, **b** rat, and **c** mouse

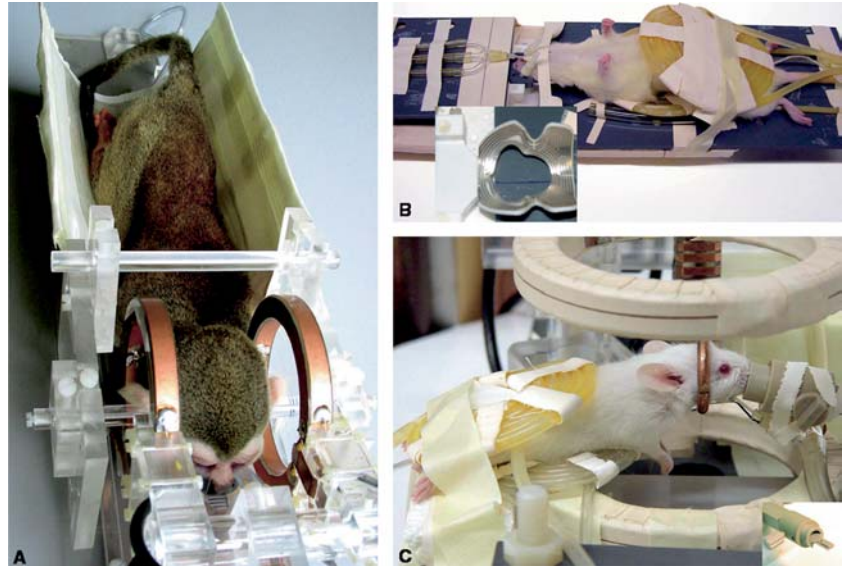
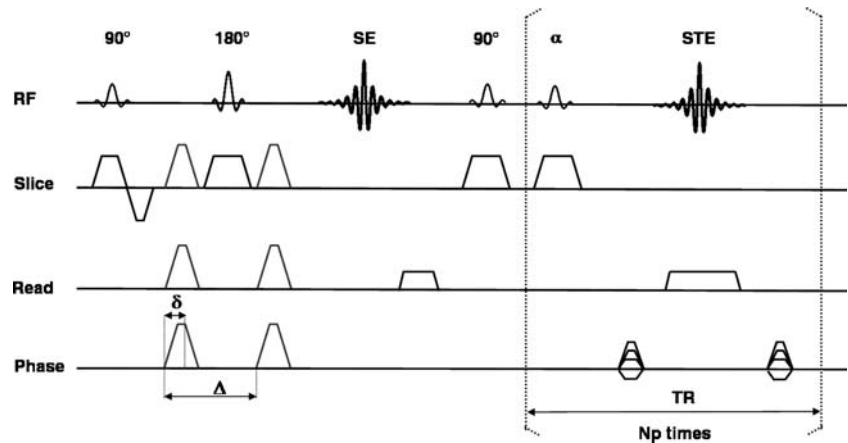


**Fig. 2** Schematic drawing of the DW single-shot STEAM MRI sequence used for diffusion tensor mapping of animal brain in vivo. The sequence combines a spin-echo (SE) preparation for diffusion encoding (gradient duration  $\delta$  and diffusion time  $\Delta$ ) with a single-shot stimulated echo (STE) imaging module using radiofrequency readout pulses with low flip angles  $\alpha$ . The brackets symbolize the repetitive readout of  $N_p$  phase-encoding steps with an internal repetition time TR



Using HF phase-encoding Eq. (1) yields

$$\alpha = \arccos \left( \exp \left( \frac{TR}{T_1} - \frac{\pi \cdot FWHM_{ph}}{FOV_{ph}} \right) \right) \quad (3)$$

with TR being the repetition time of the imaging part (see Fig. 2).

### Magnetic resonance imaging

DW single-shot STEAM MRI was implemented on a 2.35-T Bruker DBX system with B-GA20 gradients ( $100 \text{ mT m}^{-1}$ ). Apart from the acquisition of a non-DW image, DTI involved diffusion gradient encodings along six different directions (1, 1, 0; 1, -1, 0; 1, 0, 1; 1, 0, -1; 0, 1, 1; 0, 1, -1) and with three different  $b$  values of 200, 700, and  $1200 \text{ s mm}^{-2}$  in all cases. The use of a gradient pulse duration of  $\delta = 9.5 \text{ ms}$  and a diffusion time of  $\Delta = 15 \text{ ms}$  resulted in a spin-echo time for diffusion preparation which varied only slightly between  $TE = 28.45$  and  $30.75 \text{ ms}$  depending on section thickness (i.e., RF pulse duration).

After linear interpolation of the DW images to twice the matrix size, the diffusion images were Gaussian filtered with a full width at half-maximum of two pixels. Calculation of the diffusion tensor was based on a multivariate regression. To facilitate the visualization of fiber bundle orientations, maps of main diffusion direction (MDD) were color-coded and superimposed onto corresponding maps of the relative anisotropy (RA) defined according to [3]. The color code was red for right-left, green for dorsal-ventral, and blue for rostral-caudal with mixed colors for intermediate orientations. The RA maps were not thresholded by a single value. Instead, in a first step, the chosen strategy automatically accepts all pixels exceeding an upper threshold of 95% of the histogram of RA values. Subsequently, directly neighboring pixels are iteratively added until reaching a lower threshold of 65%.

Optimal imaging parameters for the single-shot STEAM MRI part were determined in a set of pilot studies on rat brain in vivo. FF and HF versions were compared using sequences at reduced spatial resolution as well as identical image acquisition

**Table 1** Comparison of full Fourier and half Fourier versions of DW single-shot STEAM MRI of rat brain in vivo using identical image acquisition (428 ms) and measurement times (28:43 min). Half Fourier phase-encoding increased both the SNR of non-DW images and the relative anisotropy (RA) contrast between six different regions of interest in the corpus callosum (CC) and cortex

	Phase-encoding steps	Flip angle (degree)	Bandwidth/Hz (pixel)	SNR	RA <sub>CC</sub> /RA <sub>Cortex</sub>
Full Fourier	48	12.7	210	11 ± 2	1.6 ± 0.3
Half Fourier	29	18.5	102	16 ± 2	2.3 ± 0.3

**Table 2** Experimental parameters for diffusion MRI of the brain of squirrel monkeys, rats, and mice using HF DW STEAM MRI in vivo

	Squirrel monkey	Rat	Mouse
Phase-encoding steps	37	45	29
Matrix	64 × 128	80 × 128	48 × 128
FOV (mm <sup>2</sup> )	44.8 × 76.8	24.0 × 25.6	13.4 × 17.9
Resolution (μm <sup>3</sup> )	700 × 600 × 1000	300 × 200 × 1500	280 × 140 × 720
TR (ms)	12.49	12.29	12.77
Flip angle (degrees)	15.4	13.2	18.4
Image acquisition time (ms)	500	590	411

(428 ms) and measurement times (28:43 min corresponding to 15 averages and an overall repetition time of 6 s). The FF version acquired 48 echoes with a bandwidth of 27 kHz (210 Hz/pixel, TR = 7.7 ms) and a flip angle of 12.7°. The corresponding HF sequence had 29 echoes with a bandwidth of only 13 kHz (102 Hz/pixel, TR = 12.7 ms) and an increased flip angle of 18.5°. Experimental comparisons were based on RA values taken from different regions of interest (ROI, 0.48 mm<sup>2</sup>) in cortex and corpus callosum (six locations each) in three different sections.

All subsequent studies of the brain of squirrel monkey, rat, and mouse ( $n = 3$  each) were performed using HF DW single-shot STEAM sequences with a bandwidth of 102 Hz/pixel and an overall repetition time for multi-slice imaging of 5 s. Together with the chosen diffusion encoding scheme which involved one non-DW image and 3 × 6 DW images, mapping of the diffusion tensor yielded a minimum measuring time of 95 s without signal averaging. In the present study, DTI acquisitions were restricted to a maximum of 3 h (110 averages) to ensure a robust handling of the anesthetized animals. Mean ADC and RA values in gray and white matter were obtained by averaging across animals ( $n = 3$ ) and ROIs ( $n = 3$ ) in cortex and corpus callosum for each species.

To allow for anatomic references, high-resolution T1-weighted 3D MRI (FLASH,  $\alpha = 25^\circ$ ) of the brain of squirrel monkeys (TR/TE = 22.3/10.1 ms), rats (TR/TE = 17.0/5.5 ms), and mice (TR/TE = 17.0/7.6 ms) were performed at 234, 230, and 117 μm isotropic resolution, respectively.

## Results and discussion

### Comparison of FF and HF DW STEAM MRI

Acquisition parameters and DTI results obtained for FF and HF versions of DW STEAM MRI are summarized

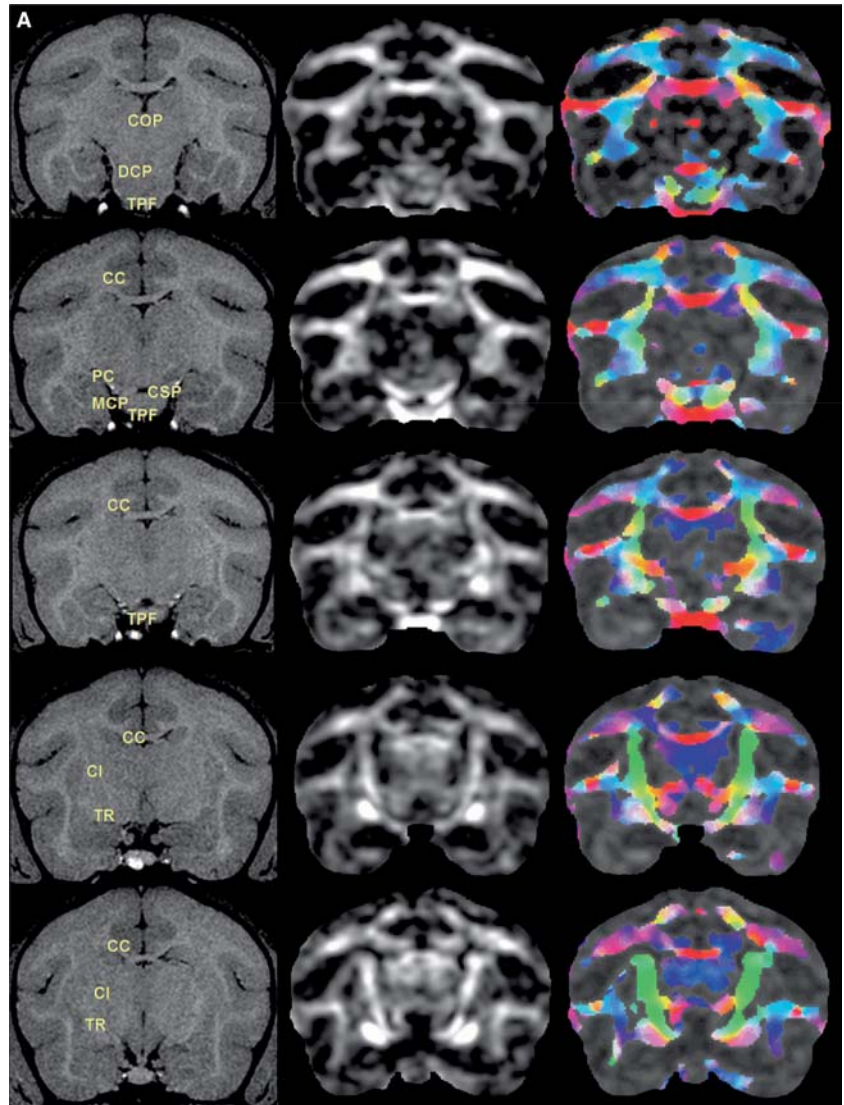
in Table 1 for rat brain in vivo. As previously suggested by non-DW STEAM MRI of human brain [21], the SNR was markedly improved by 45%. Correspondingly, the RA contrast between regions within the corpus callosum and cortex was enhanced by a similar percentage. These results confirm theoretical estimations that the use of HF phase-encoding in single-shot STEAM MRI allows for a SNR gain despite a lower number of acquired echoes. The underlying reason stems from the possibility to considerably increase the flip angle of the readout pulses (here by about 45%) and thereby proportionally increase the strength of the individual STE signals. Based on these results, all DTI studies of animal brain in vivo were performed using individually optimized HF DW single-shot STEAM MRI sequences. Using identical diffusion preparations, the experimental parameters for squirrel monkey, rat, and mouse brain are summarized in Table 2.

### DTI of squirrel monkey brain in vivo

Figure 3 compares T1-weighted anatomic images of the brain of an adult squirrel monkey with corresponding RA and color-coded MDD maps in nine consecutive sections. In accordance with a stereotaxic atlas [23], a resolution of 600 × 700 × 1000 μm<sup>3</sup> revealed all major fiber connections such as the anterior commissure, corpus callosum, and optic tract as well as thinner fibers such as the fornix and external capsule.

The specific potential of HF DW STEAM MRI is best demonstrated in the region of the brain stem where even spin-echo EPI acquisitions suffer from severe susceptibility artifacts. Fiber tracts such as the corticospinal tract and transverse pontine fibers are clearly delineated

**Fig. 3** T1-weighted anatomy (*left*), RA map (*middle*), and color-coded MDD map (*right*) of the brain of squirrel monkey in vivo in 9/10 consecutive sections from caudal (*top*) to rostral (*bottom*). (CA) Anterior commissure, (CC) corpus callosum, (CE) external capsule, (CH) optic chiasm, (CI) internal capsule, (CIN) cingulum, (COP) posterior commissure, (CSP) corticospinal tract, (DCP) decussation of superior cerebellar peduncle, (F) fornix, (MCP) middle cerebellar peduncle, (PC) cerebral peduncle, (TPF) transverse pontine fibers, (TR) optic tract



without any signal loss or geometric distortion and in excellent congruence with high-resolution MRI of the cerebral anatomy. It should also be noted that, despite a much coarser spatial resolution, DTI allows for a discrimination of nerve fiber bundles within white matter that are not discernable in the corresponding T1-weighted images. This significant gain of information in diffusion tensor mapping not only refers to the direction of fiber structures, but in some cases also relates to a better delineation of known anatomic structures such as the internal capsule (i.e., green structures in sections 4–6 of Fig. 3).

Quantitative data for ADC and RA values are summarized in Table 3. For squirrel monkey, the findings for both gray and white matter are in close agreement with literature values. For example,  $RA = 0.73 \pm 0.08$  for white matter corresponds well to  $RA = 0.65 \pm 0.05$  reported for monkeys [13]. On the other hand, a low value of

$RA = 0.14 \pm 0.05$  was found for cerebrospinal fluid (CSF) in all three species in accordance with isotropic diffusion.

#### DTI of rat brain in vivo

Similar to the data shown for squirrel monkey, Fig. 4 summarizes T1-weighted anatomic images as well as corresponding RA and MDD maps of rat brain in vivo. In the smaller brain of rats a spatial resolution of  $200 \times 300 \times 1500 \mu\text{m}^3$  allowed for the detection of major fiber connections such as the corpus callosum, hippocampal fimbria, internal and external capsule, and optic tract, consistent with a stereotaxic atlas [24].

In general, more advanced data analysis strategies that aim at tracking individual fiber connections are expected to benefit from more or less isotropic voxel dimensions. In

Fig. 3 (Contd.)

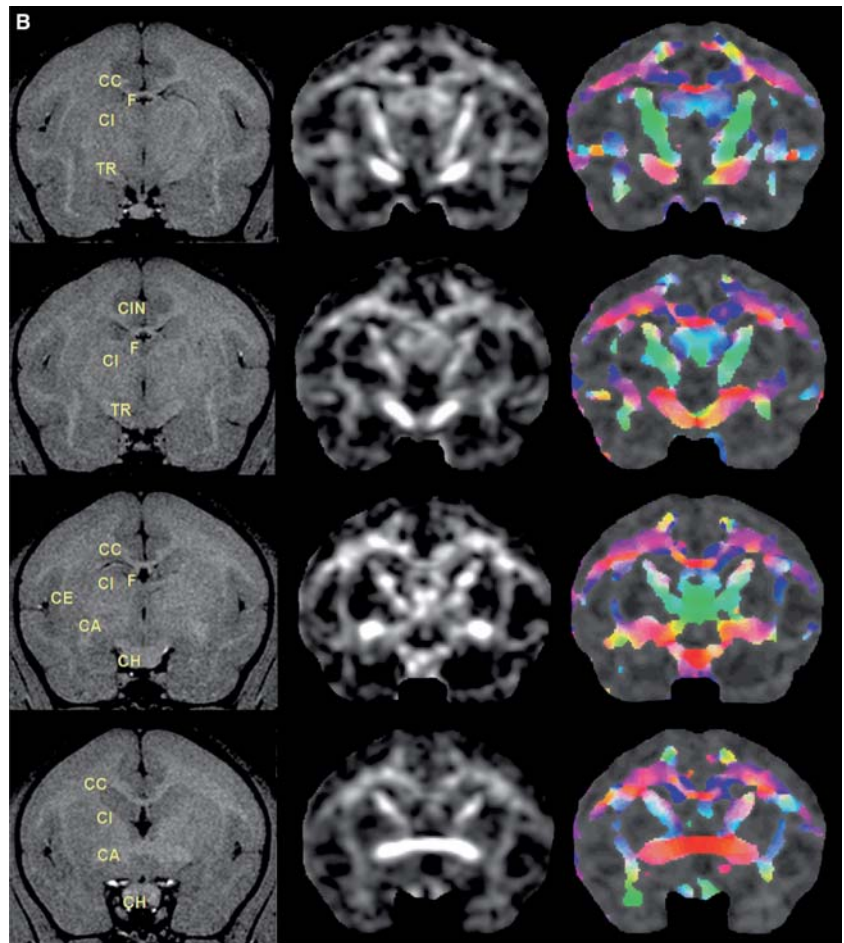


**Fig. 4** T1-weighted anatomy (*left*), RA map (*middle*), and color-coded MDD map (*right*) of rat brain in vivo in 3/8 consecutive sections from caudal (*top*) to rostral (*bottom*). (CC) Corpus callosum, (CE) external capsule, (CH) optic chiasm, (CI) internal capsule, (CIN) cingulum, (FI) hippocampal fimbria, (TR) optic tract

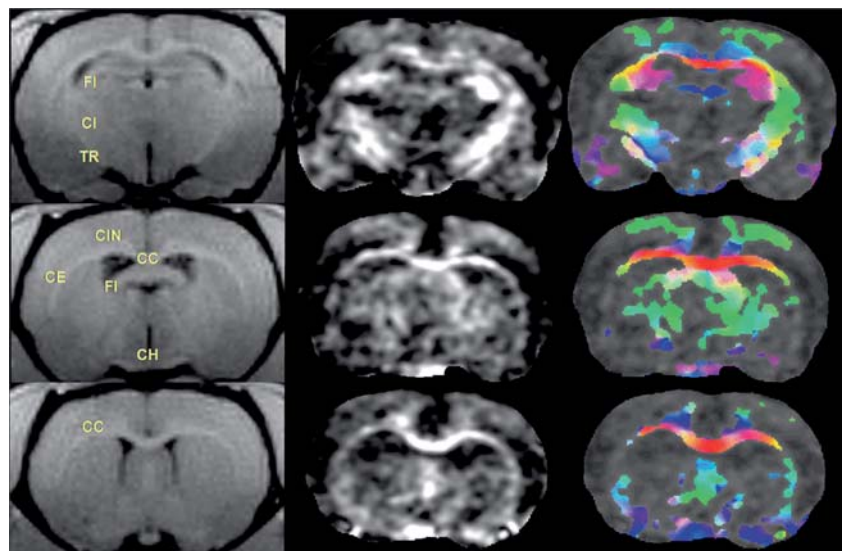
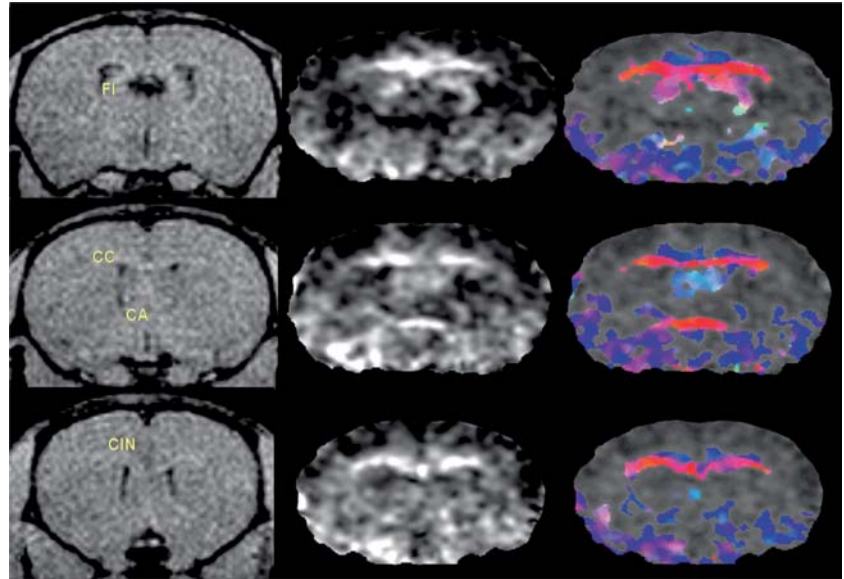


**Fig. 5** T1-weighted anatomy (*left*), RA map (*middle*), and color-coded MDD map (*right*) of mouse brain in vivo in 3/12 consecutive sections from caudal (*top*) to rostral (*bottom*). (CC) Corpus callosum, (CIN) cingulum, (FI) hippocampal fimbria, (CA) anterior commissure



the present case, however, the RA and MDD maps of rat brain demonstrate that structures that do not change their direction within a relatively thick section may be elegantly visualized by using a significantly higher in-plane resolution. The much better delineation of fiber connections in monkey (and also human) brain than in rat brain is due to the fact that the size of most nerve fiber bundles relative to the overall brain volume is much bigger in primates than in rodents. As shown in Table 3, the mean RA value of  $0.54 \pm 0.05$  obtained for white matter is lower than in primate brain but within the range of 0.5–0.8 reported previously for rat brain in vivo [15].

#### DTI of mouse brain in vivo

In the even smaller brain of mice a spatial resolution of  $140 \times 280 \times 720 \mu\text{m}^3$  turned out to be sufficient to resolve the main fiber structures of the corpus callosum, anterior commissure, and hippocampal fimbria as shown in Fig. 5 in accordance with a stereotaxic atlas [25]. Thinner structures such as the external capsule were not detectable at this resolution. Nevertheless, the corpus callosum and the anterior commissure of mouse brain are again better visualized than in anatomic T1-weighted images.

Quantitative evaluations of RA values in Table 3 yield similar results to those obtained for rats. Moreover, the RA values for CSF are identical in all species and well below the degree of white matter anisotropy. This finding suggests that the diffusion maps for mice are not contaminated by residual motion or noise contributions. In fact, a SNR problem has been avoided by adjusting the experimental conditions such as to yield similar values in all species as demonstrated in Table 3 for the non-DW images. For mice this is at the expense of higher spatial resolution.

**Table 3** SNR of non-DW images, isotropic apparent diffusion coefficients (ADC), and relative anisotropy (RA) of white and gray matter in the brain of squirrel monkeys, rats, and mice ( $n = 3$  each) achieved within a measurement time of 174 min using HF DW STEAM MRI in vivo

	Squirrel monkey	Rat	Mouse
SNR	$35 \pm 5$	$33 \pm 5$	$36 \pm 5$
ADC ( $10^{-6} \text{ mm}^2 \text{ s}^{-1}$ )			
White matter	$720 \pm 35$	$690 \pm 30$	$620 \pm 60$
Gray matter	$720 \pm 30$	$690 \pm 30$	$600 \pm 30$
RA			
White matter	$0.73 \pm 0.08$	$0.54 \pm 0.05$	$0.55 \pm 0.04$
Gray matter	$0.18 \pm 0.07$	$0.16 \pm 0.05$	$0.19 \pm 0.05$

#### Summary and conclusion

HF DW STEAM MRI allows for in vivo diffusion tensor mapping of the central nervous system in a wide range of animals from monkey to mouse and without any compromise due to motion or susceptibility artifacts. In fact, the spatial congruence of diffusion and anatomic MRI data must be considered a strong advantage (if not an essential prerequisite) for the successful application of subsequent fiber tracking analyses. Under these circumstances even the present state of diffusion tensor mapping of animal brain may provide an adequate means for the assessment of axonal damage, demyelination, or therapeutic efficacy in animal models of neurodegenerative disorders.

In a technical sense, the temporal gain of HF phase-encoding was successfully invested in a reduction of the receiver bandwidth and corresponding improvement of

the SNR which complements the signal increase caused by higher flip angles of the readout pulses. As a general result, the identification of nerve fiber bundles in RA and MDD maps of the brain of squirrel monkeys turned out to be almost comparable to DTI studies of human brain, whereas diffusion tensor recordings of the brain of mice would still benefit from a better spatial resolution.

Further improvements of DW single-shot STEAM MRI are to be expected at higher magnetic fields. In contrast to EPI-based diffusion techniques, which become even more problematic due to shorter  $T2^*$  relaxation times and enhanced magnetic field inhomogeneities, RF refocused stimulated echoes are insensitive to these effects.

Instead, DW single-shot STEAM MRI takes full advantage of the increased longitudinal magnetization and the prolonged  $T1$  relaxation times at higher magnetic fields. Finally, similar to the effects of HF phase-encoding, the SNR of DW single-shot STEAM MRI may be enhanced by a further reduction of the number of phase-encoding steps as this would allow for even higher flip angles. There are at least two foreseeable solutions to this challenge: first, the implementation of 2DRF pulses which reduce the FOV along the phase-encoding direction, and secondly, the use of parallel acquisition techniques which are not yet commercially available for animal MRI systems.

## References

- Moseley ME, Cohen Y, Kucharczyk J, Mintorovitch J, Asgari HS, Wendland MF, Tsuruda J, Norman D (1990) Diffusion-weighted MR imaging of anisotropic water diffusion in cat central nervous system. *Radiology* 176:439–445
- Chenevert TL, Brunberg JA, Pipe JG (1990) Anisotropic diffusion in human white matter: demonstration with MR techniques in vivo. *Radiology* 177:401–405
- Basser PJ, Pierpaoli C (1998) A simplified method to measure the diffusion tensor from seven MR images. *Magn Reson Med* 39:928–934
- Mori S, van Zijl PC (2002) Fiber tracking: principles and strategies – a technical review. *NMR Biomed* 15:468–480
- Beaulieu C (2002) The basis of anisotropic water diffusion in the nervous system – a technical review. *NMR Biomed* 15:435–455
- Mori S, Itoh R, Zhang J, Kaufmann WE, van Zijl PC, Solaiyappan M, Yarowsky P (2001) Diffusion tensor imaging of the developing mouse brain. *Magn Reson Med* 46:18–23
- Zhang J, van Zijl PC, Mori S (2002) Three-dimensional diffusion tensor magnetic resonance microimaging of adult mouse brain and hippocampus. *Neuroimage* 15:892–901
- Zhang J, Richards LJ, Yarowsky P, Huang H, van Zijl PC, Mori S (2003) Three-dimensional anatomical characterization of the developing mouse brain by diffusion tensor microimaging. *Neuroimage* 20:1639–1648
- Guilfoyle DN, Helpert JA, Lim KO (2003) Diffusion tensor imaging in fixed brain tissue at 7.0 T. *NMR Biomed* 16:77–81
- Choi IY, Lee SP, Guilfoyle DN, Helpert JA (2003) In vivo NMR studies of neurodegenerative diseases in transgenic and rodent models. *Neurochem Res* 28:987–1001
- Mori S, Crain BJ, Chacko VP, van Zijl PC (1999) Three-dimensional tracking of axonal projections in the brain by magnetic resonance imaging. *Ann Neurol* 45:265–269
- Parker GJ, Stephan KE, Barker GJ, Rowe JB, MacManus DG, Wheeler-Kingshott CA, Ciccarelli O, Passingham RE, Spinks RL, Lemon RN, Turner R (2002) Initial demonstration of in vivo tracing of axonal projections in the macaque brain and comparison with the human brain using diffusion tensor imaging and fast marching tractography. *Neuroimage* 15:797–809
- Pierpaoli C, Basser PJ (1996) Toward a quantitative assessment of diffusion anisotropy. *Magn Reson Med* 36:893–906
- Xue R, van Zijl PC, Crain BJ, Solaiyappan M, Mori S (1999) In vivo three-dimensional reconstruction of rat brain axonal projections by diffusion tensor imaging. *Magn Reson Med* 42:1123–1127
- Sun SW, Song SK, Hong CY, Chu WC, Chang C (2001) Improving relative anisotropy measurement using directional correlation of diffusion tensors. *Magn Reson Med* 46:1088–1092
- Song SK, Sun SW, Ramsbottom MJ, Chang C, Russell J, Cross AH (2002) Dysmyelination revealed through MRI as increased radial (but unchanged axial) diffusion of water. *Neuroimage* 17:1429–1436
- Sun SW, Song SK, Hong CY, Chu WC, Chang C (2003) Directional correlation characterization and classification of white matter tracts. *Magn Reson Med* 49:271–275
- Nolte UG, Finsterbusch J, Frahm J (2000) Rapid isotropic diffusion mapping without susceptibility artifacts: whole brain studies using diffusion-weighted single-shot STEAM MR imaging. *Magn Reson Med* 44:731–736
- Watanabe T, Michaelis T, Frahm J (2001) Mapping of retinal projections in the living rat using high-resolution 3D gradient-echo MRI with  $Mn^{2+}$ -induced contrast. *Magn Reson Med* 46:424–429
- Watanabe T, Natt O, Boretius S, Frahm J, Michaelis T (2002) In vivo 3D MRI staining of mouse brain after subcutaneous application of  $MnCl_2$ . *Magn Reson Med* 48:852–859
- Finsterbusch J, Frahm J (2002) Half-Fourier single-shot STEAM MRI. *Magn Reson Med* 47:611–615

- 
22. Rieseberg S, Frahm J (2004) Diffusion tensor imaging without susceptibility distortions using diffusion-weighted single-shot STEAM with partial Fourier acquisition. *Proc Intl Soc Mag Reson Med* 12: 1185
  23. Gergen JA MP (1963) A stereotaxic atlas of the squirrel monkey's brain (*Saimiri sciureus*). Publ. Health Service, Bethesda
  24. Paxinos G, Watson C (1998) The rat brain in stereotaxic coordinates. Academic, Orlando
  25. Rosen GD, Williams AG, Capra JA, Connolly MT, Cruz B, Lu L, Airey DC, Kulkarni K, William RW (2000) The mouse brain library. *Int Mouse Genome Conf.* @ [www.mbl.org](http://www.mbl.org).